Int. J. Solids Structures, 1974, Vol. 10, pp. 1271–1286. Pergamon Press. Printed in Gt. Britain.

COMPARISONS OF TEST AND THEORY FOR NONSYMMETRIC ELASTIC–PLASTIC BUCKLING OF SHELLS OF REVOLUTION

DAVID BUSHNELL†

Lockheed Palo Alto Research Laboratory, 3251 Hanover Street, Palo Alto, California 94304, U.S.A.

and

GERARD D. GALLETLY‡

Dept. of Mechanical Engineering, The University, Liverpool L69-3BX, England.

(*Received* 26 *December* 1973; *revised* 18 *March* 1974)

Abstract—Experimental and analytical buckling pressures are presented for very carefully fabricated thin cylindrical shells with 45, 60 and 75° conical heads and for cylindrical shells with torispherical heads pierced by axisymmetric cylindrical nozzles of various thicknesses and diameters. Nonsymmetric buckling occurs at pressures for which some of the material is loading plastically in the neighborhoods of stress concentrations caused by meridional slope discontinuities. The buckling pressures for the cone-cylinder vessels are predicted within 2·6 per cent and for the pierced torispherical vessels within 4·4 per cent with use of BOSOR5, a computer program based on the finite difference energy method in which axisymmetric large deflections, nonlinear material properties and nonsymmetric bifurcation buckling are accounted for. The predicted buckling pressures of the pierced torispherical specimens are rather sensitive to details of the analytical model in the neighborhood of the juncture between the nozzle and the head. The buckling pressures of the cone-cylinder vessels can be accurately predicted by treatment of the wall material as elastic, enforcement of the full compatibility conditions at the juncture in the prebuckling analysis, and release of the rotation compatibility condition in the bifurcation (eigenvalue) analysis.

INTRODUCTION

Numerous bifurcation buckling analyses involving plasticity have been applied to simple structures with uniform prestress. Shanley[1] and Onat and Drucker[2] studied columns; Stowell[3], Handelman and Prager[4], and Gerard and Becker[5], investigated plates; and Bijlaard[6], Batterman[7], Jones[8], Hutchinson[9], and others[10] treated shells. Recently Lee[11] calculated bifurcation buckling pressures of elastic–plastic ring-stiffened cylinders, including nonlinear and nonuniform prebuckling stress states. Hutchinson[12] gives an excellent survey of the field, providing a firm, rational foundation for the application of bifurcation buckling analysis to predict the failure of practical shell structures.

With the high speed digital computer it is now feasible to calculate elastic–plastic bifurcation buckling loads of rather complex shell structures. In[13] Bushnell gives the nonlinear axisymmetric prebuckling theory for segmented, branched shells of revolution and in[14] the analysis for nonsymmetric bifurcation buckling is presented. The purpose of this paper is to provide evaluation of these analyses by comparison with tests of very carefully fabricated vessels submitted to uniform external pressure. Two series of tests were conducted, the first on six torispherical heads with axisymmetric nozzles (Fig. 1), and the second on three cone–cylinder vessels (Fig. 9).

† Staff Scientist. ‡Professor.

FABRICATION, MEASUREMENT AND TESTING OF THE SPECIMENS

The vessels were fabricated by the Department of Mechanical Engineering at The University in Liverpool, England. All specimens were machined from solid billets of aluminium alloy. For accuracy a copying attachment was used on a lathe. The male and female templates for the specimens were produced from gauge plate with use of a high-precision jig boring technique. The machining procedure adopted was:

(a) Machine billets down to within 0·1 in. of the final size on both inside and outside surfaces, in that order.

(b) Subject each component to a quenching heat treatment selected so as to minimize distortion and the formation of residual stresses.

(c) Fine-machine each component on the inside and then on the outside surfaces, taking comprehensive dimensional checks before and after the final cuts.

On completion of machining each vessel was subjected to a detailed thickness and diameter survey. The circularity of the vessels at different locations was also checked with use of an air bearing out-of-roundness measuring instrument. All diameters were correct to within 0·15 per cent and circularity, defined by $(a_{max} - a_{min})$ where "a" is the radius, was maintained to within 0·003 in. The variation in thickness of the cone-cylinder specimens was $\pm$0·001 in. and the thickness distribution in the pierced torispherical specimens is given in Table 1. (The thickness is assumed to vary linearly between stations where it is specified). No measurements were taken to indicate the location of the middle surface, but in the analysis it was assumed that this surface corresponds exactly with the nominal dimensions given in Figs. 1–3. The radius of the nozzle for Specimens A1 and A2 was 0·27 in.

Material properties were determined from tensile specimens which were machined oversize from the billets of the two materials involved, heat treated concurrently with the vessel components, and given a final machining. Stress–strain data thus determined are given in Fig. 2 for the torispherical specimens and Fig. 10 for the cone–cylinder vessels.

The pierced torispherical shells were supported as shown in Fig. 1. The seal was made pressure-tight by application of a non-setting joining compound in the groove before insertion of the vessel. For specimens of this geometry reasonable variations in the fixity of the large-diameter cylinder have negligible effect on the predicted buckling loads, since failure occurs near the juncture between the nozzle and head.

Table 1. Thickness distribution in pierced torispheres
(all dimensions in inches)

Location†	Arc length	Specimens A1	A2	Arc length	Specimens A3	A4	Arc length	Specimens A5	A6
Beginning of Segment 1	0·0	0·027	0·054	0·0	0·027	0·055	0·0	0·0270	0·0540
Begin. 2							1·300		0·0540
Begin. 2	1·400	0·028	0·054	1·400	0·028	0·055	1·400	0·0270	
End 2	1·473	0·028	0·054	1·473	0·028	0·055	1·473	0·0280	0·0550
Begin. 3	1·473	0·056	0·056	1·473	0·055	0·056	1·473	0·0550	0·0550
Begin. 4	2·233	0·053	0·053	1·820	0·050	0·052	1·810	0·0531	0·0530
Begin. 5	3·116	0·053	0·053	2·710	0·050	0·052	2·290	0·0531	0·0505
End 5	4·561	0·053	0·053	4·150	0·050	0·052	3·735	0·0525	0·0510
Begin. 6	4·561	0·052	0·052	4·150	0·052	0·052	3·735	0·0525	0·0520
End 6	5·911	0·052	0·052	5·500	0·052	0·052	5·085	0·0525	0·0520

† See Figs. 2 and 3 for indication of segment boundaries.

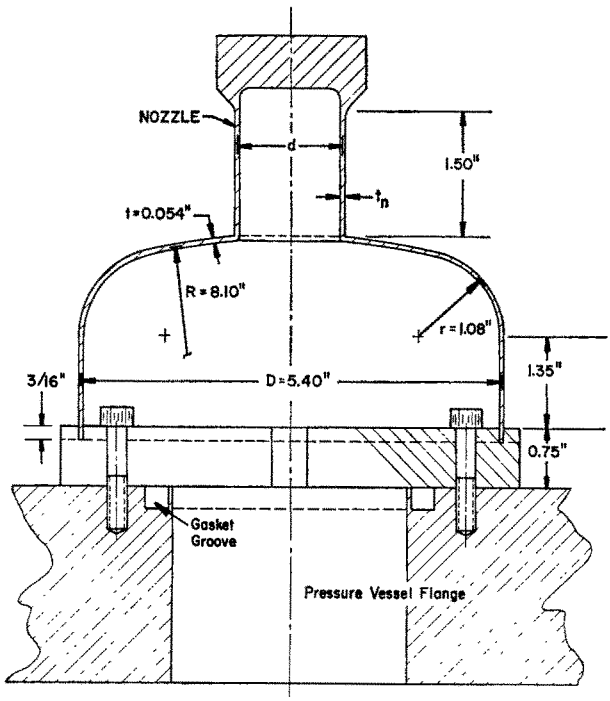

Fig. 1. Torispherical head with axisymmetric nozzle.

The symmetrical cone–cylinder vessels were constructed with the use of two identical half-vessels. The use of complete vessels, with a symmetry plane at which conditions are known, is necessary for the geometries investigated because certain failure modes involve the cylindrical portion. Several techniques were considered for joining the two half-vessels. However, only two appeared practical—welding and the use of adhesives. The disadvantage of welding is that the metal near the joint is degraded by localized heating, leading to an unknown change in material properties. Welding also introduces residual stresses and associated dimensional errors. With use of adhesives these penalties are not incurred, but the adhesive joint fails during the buckling process, thereby preventing experimental verification of the predicted bifurcation buckling mode shape. The mating faces of the two halves of each vessel were machined to give a flat butt joint and after thorough degreasing were glued together with a common Araldite adhesive. Alignment during gluing and curing was assured by holding each half in one of a pair of perspex flanges previously bored to match the outside diameters of the cylinders. The perspex flanges had been bored together. Four dowel pins inserted through the two flanges ensured the necessary alignment.

The tests were conducted in a 6 in. dia. pressure vessel, flanged at one end. Water was the pressurizing medium. Pressure measurement was accomplished by a strain gauge type pressure transducer with a conventional dial gauge used for order-of-magnitude checks.

TORISPHERICAL HEADS WITH AXISYMMETRIC NOZZLES

Figure 1 shows the geometry with nominal dimensions. The actual thickness distributions along the walls of the 6 specimens are given in Table 1. The heavy section at the top of the nozzle was modeled in BOSOR5 as a very stiff ring. The nozzle dia d and thickness t_n vary

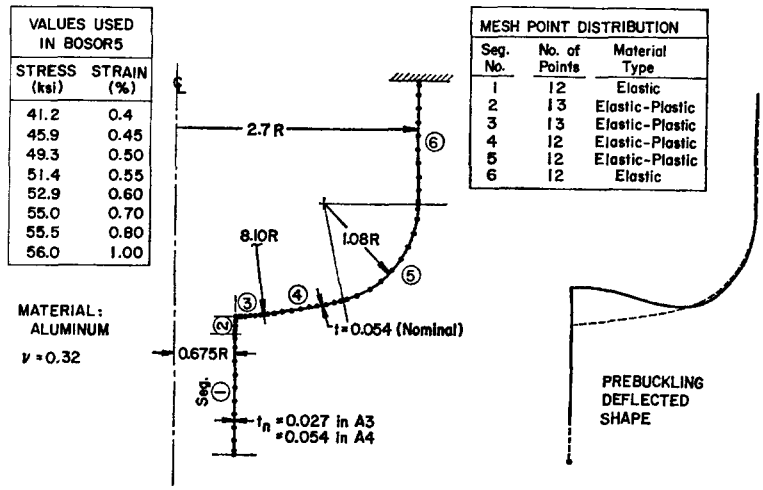

Fig. 2. Discrete model of specimens A3 and A4 with material properties and exaggerated prebuckling deflected shape.

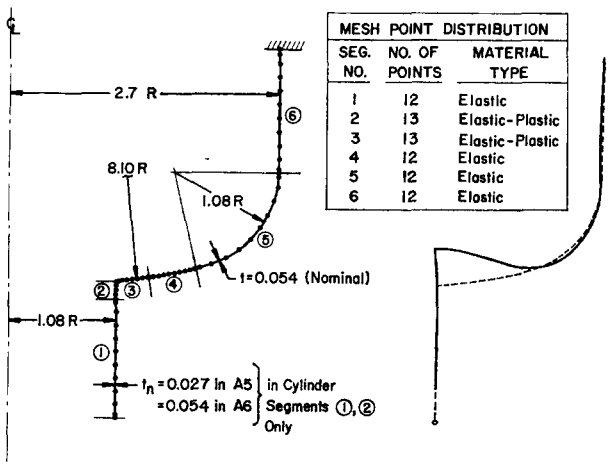

Fig. 3. Discrete model of specimens A5 and A6 with exaggerated prebuckling deflected shape.

from specimen to specimen. Figures 2 and 3 give the mesh point distributions and the dimensions of the nozzle for Specimens A3–A6. In BOSOR5 the uniaxial stress–strain curve is modeled as a series of straight line segments connecting the material data points specified in Fig. 2.

Initial computer runs were made with no plasticity in order to determine the optimum distribution of nodal points and division of the shell into segments. (Computer time is saved if entire segments of the structure can be treated as elastic). Prebuckling deflections (not to scale) are shown in Figs. 2 and 3 and the extreme fiber meridional and hoop strain distributions in Specimen A4 are shown in Fig. 4. From preliminary computer runs it became obvious that prior to buckling only a very small amount of plastic flow occurs near

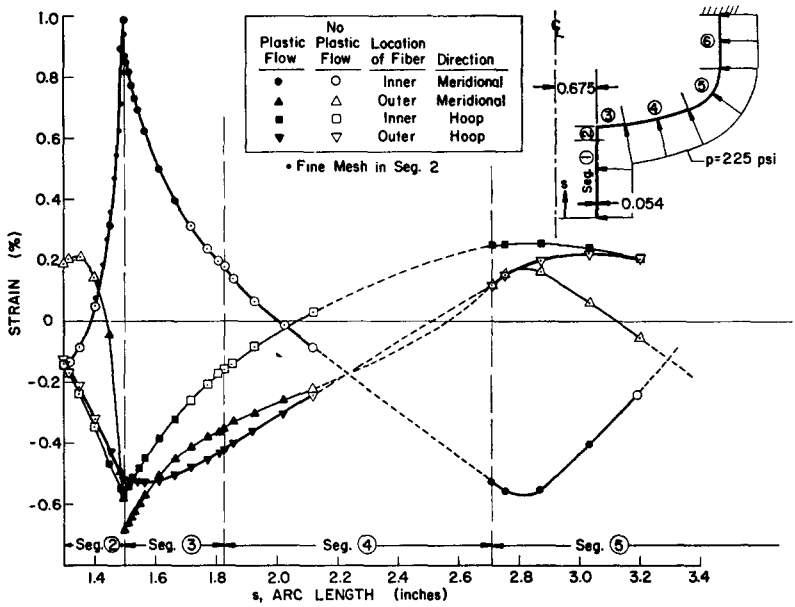

Fig. 4. Predicted extreme fiber meridional strain distribution in specimen A4 with use of model C (see Fig. 6).

Table 2. Experimental and theoretical buckling pressures for the torispherical heads with axisymmetric nozzles

Case	Description of model	Buckling pressures (psi) A1	A2	A3	A4	A5	A6
1	Experimental results	257	260	177	208	168	215
2	Elastic–plastic in segments 2 and 3, actual thickness†, model A‡	—	—	182	205	160	206
3	Elastic–plastic in segments 2 and 3, nominal thickness§, model A	—	—	179	—	160	—
4	Elastic–plastic in segments 2–5, actual thickness, model A	256	256	—	—	—	—
5	Same as case 2, except deformation theory used	—	—	—	—	—	205
6	Same as case 2, except elastic shear modulus used	—	—	—	—	—	270
7	Elastic–plastic in segments 2 and 3, nominal thickness, model B	—	—	—	—	159	—
8	Elastic–plastic in segments 2 and 3, nominal thickness, model C	—	—	164	227	148	221
9	Same as case 8, except elastic–plastic in segments 2–5	—	—	—	225	—	—
10	Elastic in all segments, actual thickness distribution, model A	264	264	217	221	228	269
11	Same as case 10, except with hinge at nozzle-head juncture in both prebuckling and stability analyses	—	—	128	123	115	112
12	Same as case 10, except with hinge at nozzle-head juncture in the stability analysis only	—	—	181	184	174	197

† The actual thickness distributions are given in Table 1. Thicknesses are presumed to vary linearly between data points.
‡ Models A, B and C are identified in Figure 6.
§ The nominal thickness in the nozzle is 0·027 in. in A1, A3, and A5; 0·054 in. in A2, A4 and A6. In the rest of the structure the nominal thickness is 0·054 for all specimens. The diameter of the nozzle measured to the middle surface is 0·54 in. in specimens A1 and A2; 1·35 in. in A3 and A4; and 2·16 in. in A5 and A6.

the juncture between segments 4 and 5 in specimens A4 and A6 and none at all at this location in specimens A3 and A5. Hence these segments, as well as segments 1 and 6, were considered to be elastic in subsequent runs for these specimens. In the case of specimens A1 and A2, segments 2–5 were considered to be elastic–plastic.

Table 2 gives the critical pressures from tests and theory. In all cases the minimum critical pressure corresponds to one circumferential wave: during buckling the nozzle gradually tilts to one side. Predicted buckling modes are shown in Fig. 5. The modes for specimens A1 and A2 are similar. This $n = 1$ mode of failure was consistently observed in the tests, even though the corresponding predicted critical pressure is only a few per cent below the predicted axisymmetric collapse pressures in every case.

The analytical predictions are rather sensitive to the modeling of the shell at the juncture between the nozzle and the head. Figure 6 shows three ways of treating the juncture. In model A the two points separated by radial and axial distances d_1 and d_2 are considered to be connected by a rigid link, free to translate and rotate but not to stretch. In model B the reference surfaces are the outer surfaces and the end point of segment 2 is connected to the third point in segment 3. In model C the middle surfaces are connected together. From Table 2 it is seen that the critical pressures predicted with models A and B are almost equal. The critical pressure predicted with model C is considerably lower in the only examples (A3 and A5) for which both model A and model C were investigated with the same nominal thickness distributions.

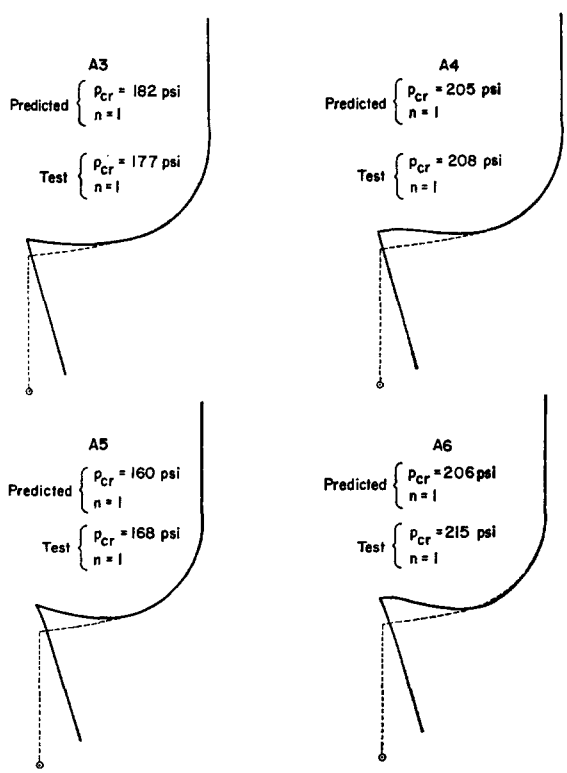

Fig. 5. Predicted bifurcation buckling mode shapes for specimens A3–A6.

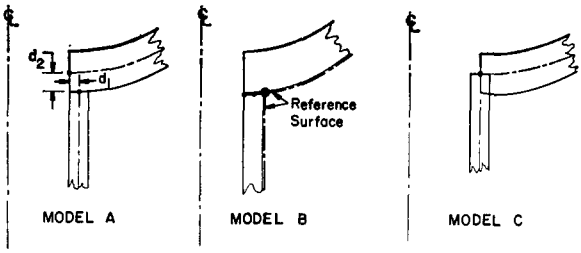

Fig. 6. Various models of the nozzle-head juncture.

The difference is explained somewhat by Figs. 7 and 8, which correspond to the prebuckling solution at a pressure of 140 psi. In model C, segment 2, the short section of nozzle immediately adjacent to the head, deforms locally a considerable amount within 1/2 the thickness of segment 3. This physically impossible situation is avoided in both models A and B, for which considerably less prebuckling deformation occurs at a given pressure because a certain length of rather flexible thin-walled material has been replaced by a shorter length of relatively stiff thicker-walled material. (Note, however, that all three models contain the same total amount of material at the juncture). Figure 7 shows the local distortion near the juncture predicted with models A and C. The points of intersection of the middle surfaces have been superposed for the two cases in order to provide a better comparison of the relative amounts of distortion and rotation of the juncture. Actually, at $p = 140$ psi the predicted axial movement of this point is 0·04283 in. for model A and

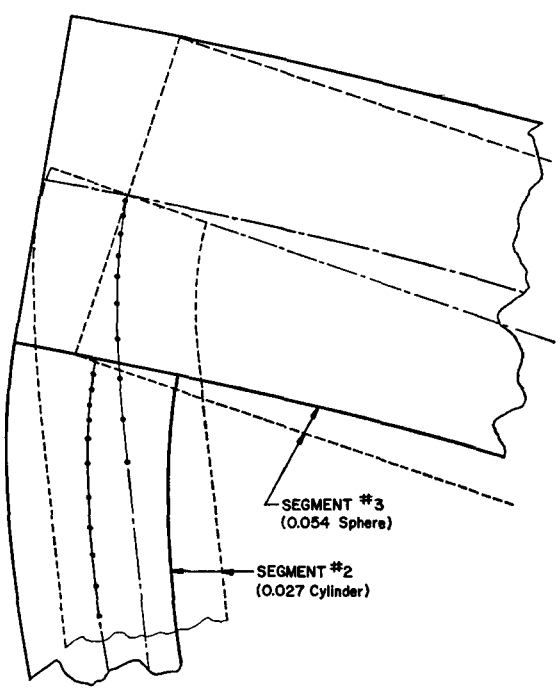

Fig. 7. Local distortions of specimen A5 at the nozzle-head juncture at $p = 140$ psi, predicted with use of models A and C.

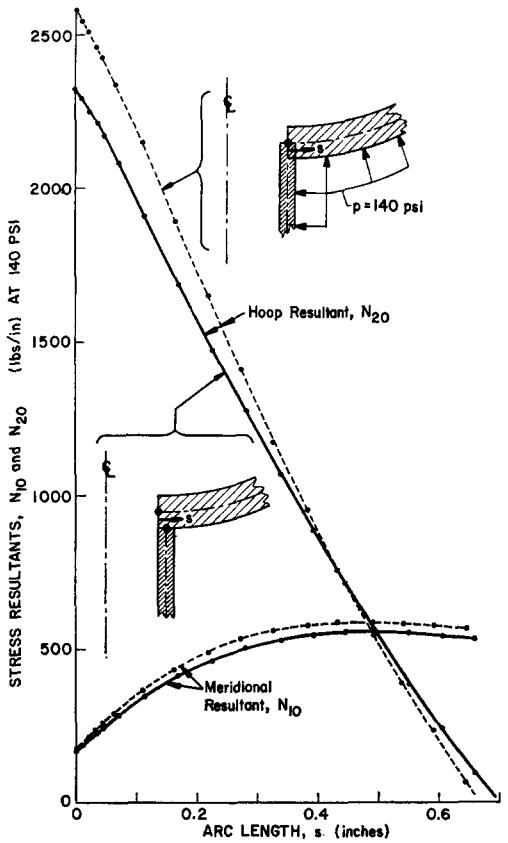

Fig. 8. Prebuckling stress resultants in specimen A5 obtained with models A and C.

0·05232 in. for model C. The meridional rotation is 2·09° for model A and 3·51° for model C. Figure 8 shows that at the given pressure model A leads to slightly lower stress resultants in segment 3, where the buckling amplitude is relatively large.

To summarize—the predicted buckling pressure is higher for model A than for model C for two reasons:

(1) The destabilizing prestresses are lower at a given pressure, and
(2) The structure is stiffer so that even if the prestresses were the same at a given pressure, the bifurcation pressure would be higher for model A than for model C.

Even with the stiffer model A there is considerable local distortion immediately adjacent to the juncture. A very accurate analysis of the buckling of this vessel requires the inclusion of transverse shear deformations in this area. Thin shell theory is simply not adequate. This fact and the fact that the predicted buckling pressures are quite sensitive to the way in which this local area is modeled tend to lead to the conclusion that the good agreement between test and theory is somewhat fortuitous.

Notice in Table 2 that the predicted bifurcation buckling pressures are lower than the test values for five of the six specimens. If the analysis and the test specimens were perfect, this result would be expected because bifurcation buckling analysis of a structure loaded into the plastic range of material behavior leads to a slight underestimation of the collapse load.

Shanley has shown this for the column and Hutchinson for the spherical shell. These authors and others have demonstrated that the initial postbuckling load–deflection curve has a positive slope and that the maximum load-carrying capacity is therefore slightly above the bifurcation point. However, in the tests and analysis described here various effects such as geometrical imperfections, residual stresses, and unknown variation of material properties, in addition to the neglect of transverse shear deformations, would be expected to contribute errors in the predicted critical pressures at least as large as the discrepancies between test and theory actually obtained.

Notice that for specimens A1 and A2 the predicted buckling load is independent of the nozzle thickness. This result is reasonable because the nozzle is only one-tenth the diameter of the head in these cases. Also, notice that the effect of plasticity is small for A1 and A2.

While no analytical prediction of the sensitivity to imperfections is given here, the close agreement between test and theory even for specimens in which not much plastic flow occurs indicates that imperfections are not too significant for these configurations. The reader should not draw the conclusion from these limited results that buckling loads for all shells will be less sensitive to imperfections if buckling occurs after the material has yielded. On the contrary, one would expect for certain configurations, such as a spherical shell under external pressure or a cylinder under axial compression, that the presence of nonlinear material behavior might increase the sensitivity to imperfections: if local plastic flow occurs because of local bending in the neighborhood of a dimple, the dimple will grow faster with increase in load than it would have if the material had remained elastic.

On the other hand, if the stress–strain curve has a sharp "knee" and if the wall material is stressed well beyond the proportional limit in regions of the shell which are relatively free of bending, buckling will occur because of general "softening" of the material, not because of local growth of an imperfection. The buckling load in such a case can be predicted from a simple stress or limit analysis—the shell collapses when it becomes a mechanism because of unconstrained plastic flow.

Intermediate between the situation involving growth of a local plastic dimple and that involving general plastic failure, is the situation in which the essential effect of plastic flow is to alter the stiffness in a predictable way at stress concentrations such as clamped boundaries or meridional discontinuities. For example, high bending stresses at a clamped boundary cause the material to yield, leading to a constraint condition in the stability analysis that may resemble simple support more than clamping. If the predicted buckling load is sensitive to this *predictable* change in stiffness, the effect will generally be to reduce its sensitivity to the *unknown* geometric imperfections. Buckling is caused by the predictable "relaxation" of a constraint due to plastic flow, not by the growth of a geometric anomaly.

The cases studied in this paper exemplify this intermediate situation. During loading most of the plastic flow is confined to small axisymmetric regions near the sharp slope discontinuities between the nozzles and the spherical heads. Cases 11 and 12 in Table 2 represent attempts to model A3–A6 as elastic and to account for the plasticity by introduction of a hinge at the nozzle-head juncture. Case 12 apparently represents a reasonably good model of the actual system. More is said about these alternative elastic models in the next section.

CONE–CYLINDER VESSELS

Figure 9 shows the three configurations investigated. In the analysis the inner surface was used as a reference surface and there was no elaborate treatment of the corners. The apex of the cone was replaced by a hole of 0·1 in. radius with the edge of the hole considered

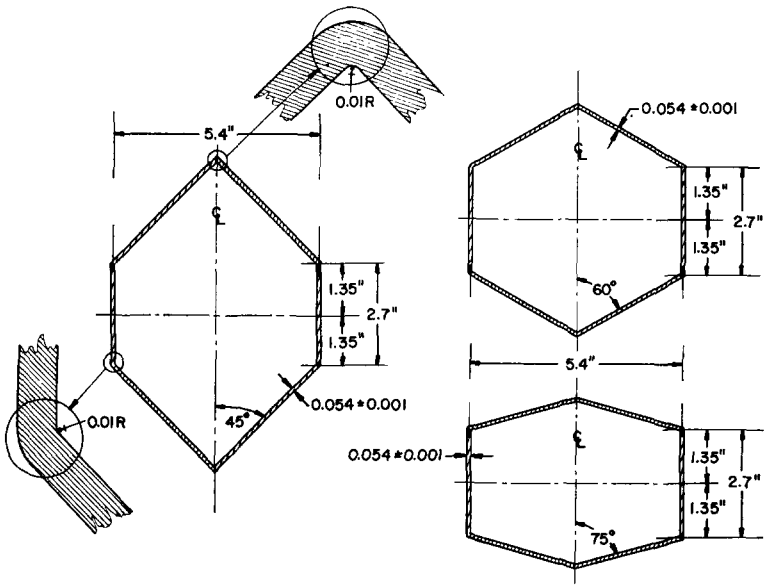

Fig. 9. Cone–cylinder specimens.

to be free. Figure 10 gives the experimentally determined stress–strain behavior of four tensile specimens processed in the same way as the vessels. Only the two extreme curves were used in the analysis.

As in the case of the torispherical heads, an elastic analysis was first undertaken in order to determine the optimum distribution of nodal points and division of the shell into segments. Figures 11 and 12 show the discrete models A and B.

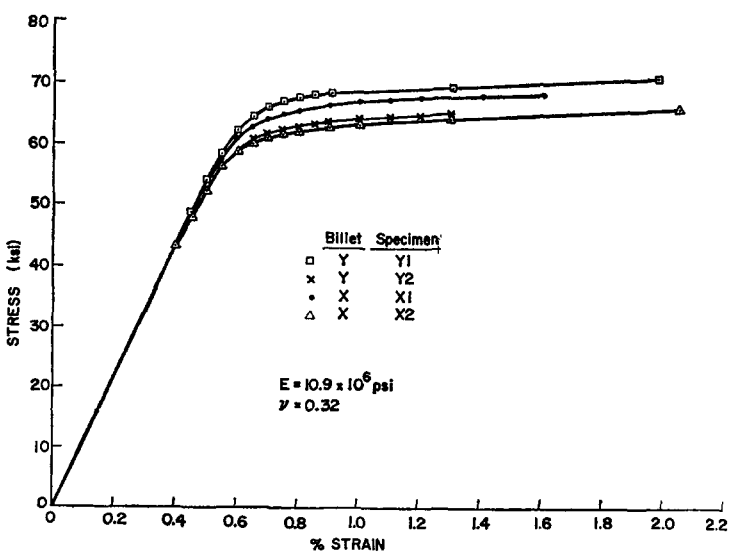

Fig. 10. Material properties for cone–cylinder specimens.

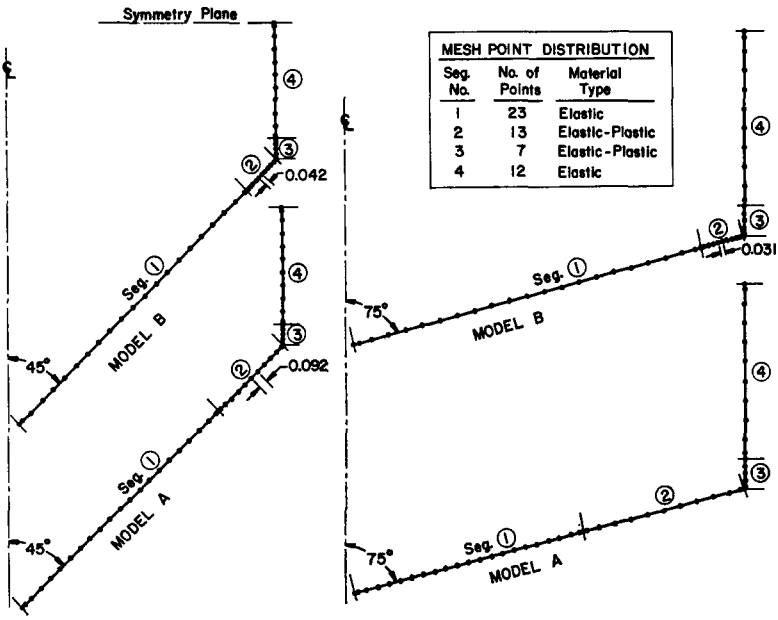

Fig. 11. Discrete models of the 45 and 75° specimens.

The experimental and analytical results are given in Table 3. The predictions from the most refined models correspond to cases 2 and 3. It is seen that for the configurations investigated a good elastic model is one in which meridional moment compatibility at the cone–cylinder juncture is enforced in the prebuckling analysis but relaxed in the stability analysis (case 6). That the predicted buckling loads are close to the test values for this simplified elastic model apparently is the result of two counteracting errors: The prebuckling

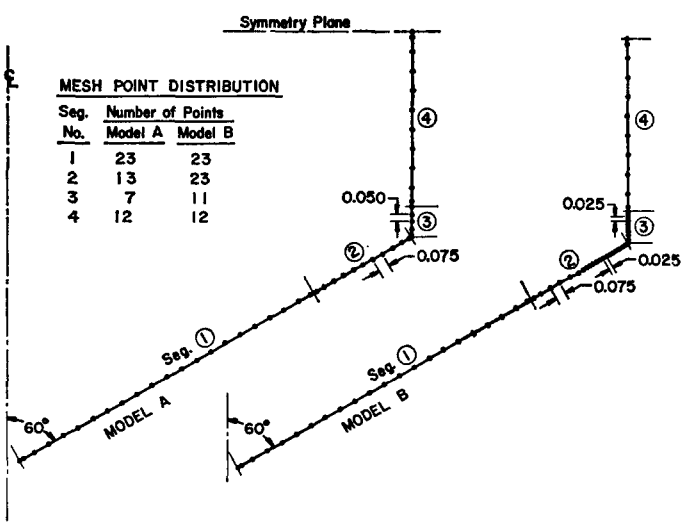

Fig. 12. Discrete models of the 60° specimen.

Table 3. Experimental and theoretical buckling pressures of cone–cylinder vessels

Case	Description of model	Buckling pressures (psi) 45°	60°	75°
1	Experimental results	559	410	185
2	Elastic–plastic, model B†, billet x, spec. $x2$‡	553(6)§	397(3)	184(2)
3	Elastic–plastic, model B, billet y, spec. $y1$	561(6)	408(3)	190(2)
4	Elastic–plastic, model A, billet x, spec. $x2$	549(6)	396(3)	183(2)
5	Elastic–plastic, model B, billet x, spec. $2x$ with use of J_2 deformation theory rather than J_2 flow theory	552(6)	—	—
6	Same as case 2, except with use of elastic shear modulus in stability analysis	556(6)	—	—
7	Elastic ($E = 10{\cdot}9 \times 10^6$ psi) with juncture hinge in stability analysis only, model A	564(6)	434(4)	185(2)
8	Elastic with hinge in both prebuckling and in stability analysis, model A	509(6)	327(4)	113(2)
9	Elastic with no hinge at all, model A	598(6)	473(4)	213(2)

† Models A and B are shown in Figs. 11 and 12.
‡ Stress–strain curves for four tensile specimens are given in Fig. 10. The two specified in this table represent the extremes.
§ Numbers in parentheses are the number of circumferential waves corresponding to the lowest predicted bifurcation buckling pressure.

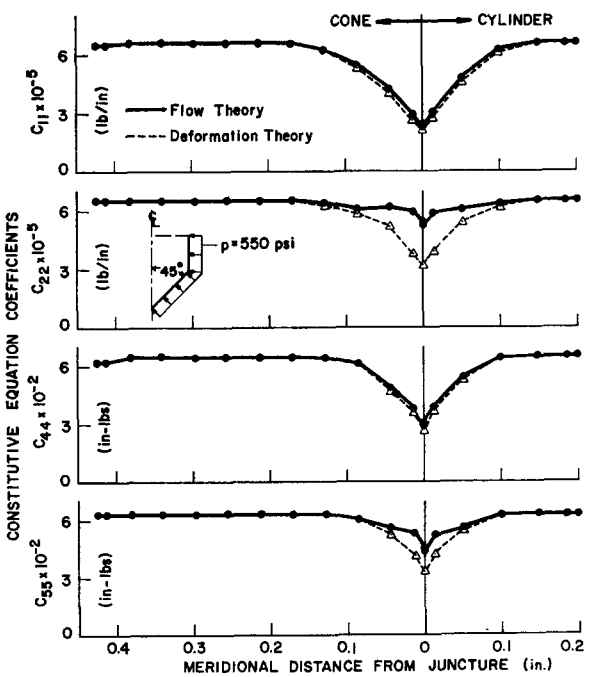

Fig. 13. Integrated meridional (C_{11} and C_{44}) and hoop (C_{22} and C_{55}) extensional and bending stiffnesses at 550 psi in the 45° specimen.

model is too stiff and therefore at a given pressure the stress resultants, which appear in the stability equations, are too small. Counteracting this effect is the underestimation of the meridional bending rigidity at the juncture in the stability analysis. Clearly both effects are important, since introduction of the hinge in the prebuckling analysis lowers the predicted buckling pressure considerably, and enforcement of elastic meridional moment compatibility in the stability analysis raises it considerably.

One calculation (case 5) was made with the use of J_2 deformation theory. The critical pressure is very slightly different from that obtained with J_2 flow theory, although as seen in Fig. 13 the constitutive equation coefficients C_{22} (hoop extensional rigidity) and C_{55} (hoop bending rigidity)[14] are quite different at a pressure of 550 psi. In both the flow theory and deformation theory analyses the value of the shear modulus predicted by deformation theory is used in the stability equations. The reasoning behind this strategy is given in [14]. Use of the elastic shear modulus in the otherwise unchanged case 2 yields a predicted buckling pressure of 556 psi. A similar parameter study is performed for one of the torispherical heads and results are listed in Table 2 as cases 5 and 6.

Figure 14 shows the effect on the meridional bending stiffness, C_{44}, of varying the number of integration points through the thickness of the shell. (The elastic values which these curves approach are slightly different from those shown in Fig. 13 because the material

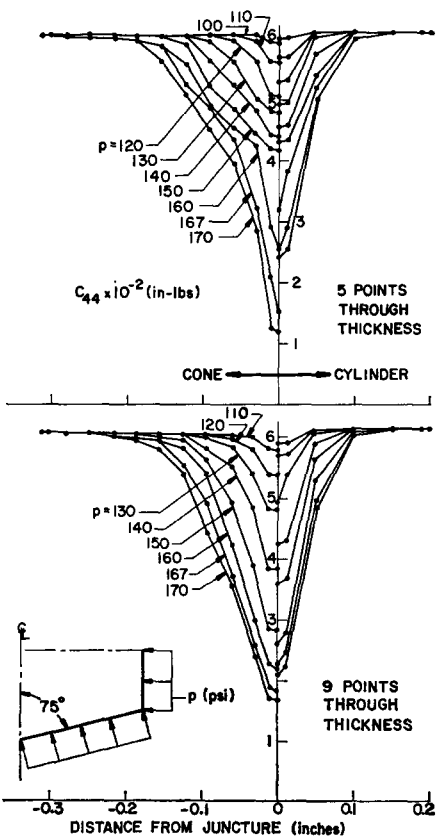

Fig. 14. Integrated meridional bending stiffness C_{44} for 5 and 9 integration points through the shell wall thickness.

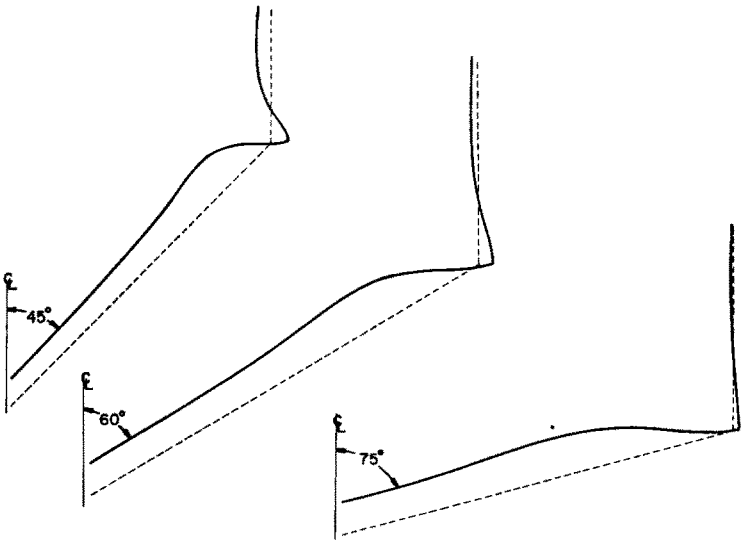

Fig. 15. Exaggerated prebuckling deflected shapes for the three cone–cylinder specimens.

properties are given in Fig. 2 rather than Fig. 10.) With 9 integration points the distributions are more smoothly varying. This effect, however, is not important as far as the prediction of buckling pressure is concerned, leading to changes only in the fourth significant figure in the examples studied.

Figure 15 shows in exaggerated form the prebuckling deflections of the three specimens, and Figs 16–18 show the predicted bifurcation buckling modes for cases 2, 8 and 9.

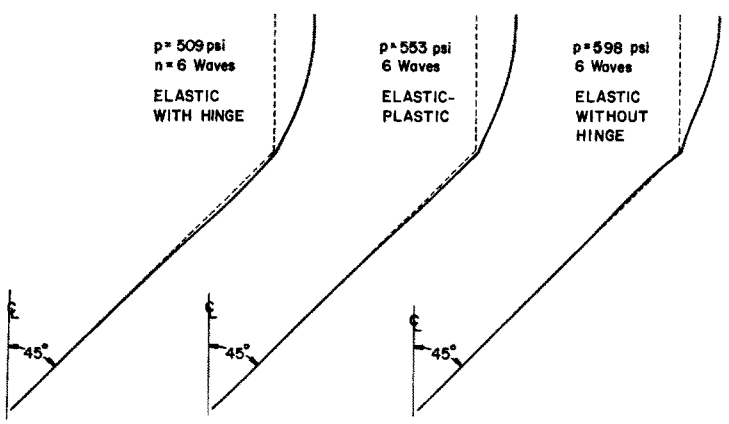

Fig. 16. Buckling modes for the 45° specimen corresponding to cases 2, 8 and 9 in Table 3.

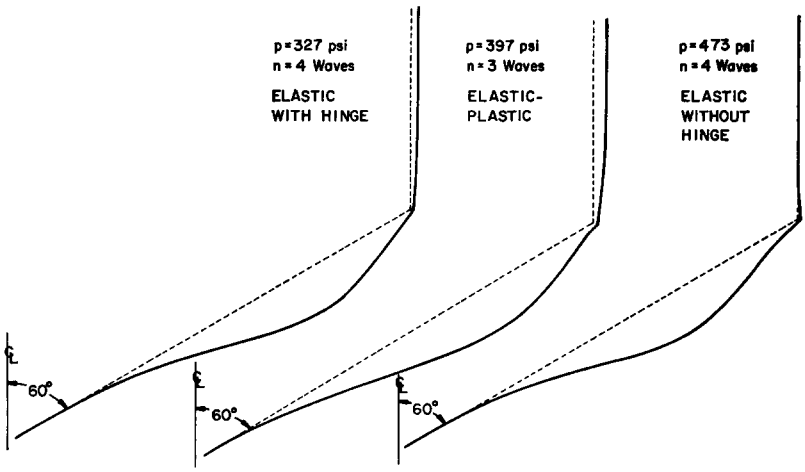

Fig. 17. Buckling modes for the 60° specimen corresponding to cases 2, 8 and 9 in Table 3.

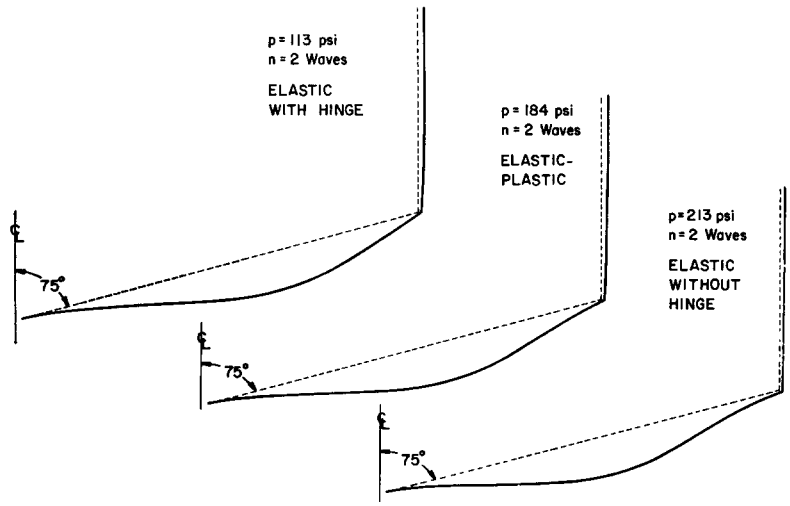

Fig. 18. Buckling modes for the 75° specimen corresponding to cases 2, 8 and 9 in Table 3.

CONCLUSIONS

In every example treated here the significant plasticity is confined to a local region near a meridional slope discontinuity. Local plastic flow is caused primarily by a combination of hoop membrane strain and meridional bending strain, with the latter being the more significant. The single most important effect of the plasticity in the cases studied is to create a partial hinge at the meridional slope discontinuities. The hinge causes increased compressive prebuckling stress resultants at given pressures and reduced stiffness coefficients in the stability equations, both effects leading to reductions in the prediction of the bifurcation load from what it would be with use of a theory involving only elastic behavior.

The differences between predictions with use of J_2 flow theory (in which the effective shear modulus is the value from J_2 deformation theory) and predictions with use of J_2 deformation theory are very small in the cases studied. Also, the results are insensitive to variation of the shear modulus.

While good agreement was obtained between test and theory for the torispherical heads, it is clear that transverse shear deformations should be accounted for in the neighborhood of the nozzle-head juncture. Since the predicted bifurcation buckling pressures are sensitive to details in the discrete modeling of this area, and since the important effect of transverse shear deformations is neglected in the thin shell analysis on which BOSOR5 is based, it is felt that the good correlation in the case of the torispherical heads is somewhat fortuitous.

Acknowledgement—The analytical portion of this work was supported by the Lockheed Independent Research Program.

REFERENCES

1. F. R. Shanley, Inelastic Column Theory, *J. Aero. Sci.* **14**, 261 (1947).
2. E. T. Onat and D. C. Drucker, Inelastic Instability and Incremental Theories of Plasticity, *J. Aero. Sci.* **20**, 181 (1953).
3. E. Z. Stowell, A Unified Theory of Plastic Buckling of Columns and Plates, *NACA TN* 1556 (April 1948).
4. G. H. Handelman and W. Prager, Plastic Buckling of a Rectangular Plate Under Edge Thrusts, *NACA TN* 1530 (Aug. 1948).
5. G. Gerard and M. Becker, Handbook of Structural Stability: Part I—Buckling of Flat Plates, *NACA TN* 3781 (1957).
6. P. P. Bijlaard, Theory and Tests on the Plastic Stability of Plates and Shells, *J. Aero. Sci.* **16**, 529 (1949).
7. S. C. Batterman, Tangent Modulus Theory for Cylindrical Shells: Buckling Under Increasing Load, *Int. J. Solids Struct.* **3**, 501 (1967).
8. R. M. Jones, Plastic Buckling of Eccentrically Stiffened Circular Cylindrical Shells, *AIAA Journal* **5**, 1147 (1947).
9. J. W. Hutchinson, On the Postbuckling Behavior of Imperfection-Sensitive Structures in the Plastic Range, *J. Appl. Mech.* **39**, 155 (1972).
10. M. J. Sewell, A survey of Plastic Buckling, *Stability*, edited by H. Leipholz, Chap. 5, p. 85 (1972).
11. L. H. N. Lee, General Elastic–Plastic Instability of Ring-Stiffened Cylindrical Shells Under External Pressure, *University of Notre Dame Technical Report* No. SM156 (Feb. 1973).
12. J. W. Hutchinson, Plastic Buckling, *Advances in Applied Mechanics*, edited by C. S. Yih, Vol. 14. Academic Press (1974).
13. D. Bushnell, Large Deflection Elastic–Plastic Creep Analysis of Axisymmetric Shells, *Numerical Solution of Nonlinear Structural Problems*, AMD-Vol. **6**, p. 103 (1973) (Published by the ASME).
14. D. Bushnell, Bifurcation Buckling of Shells of Revolution Including Large Deflections, Plasticity and Creep, *Int. J. Solids Struct.* **10**, 1287 (1974).